Stem Cell Reports

Article

Macroencapsulated Human iPSC-Derived Pancreatic Progenitors Protect against STZ-Induced Hyperglycemia in Mice

Corinne Haller,[1,9] Julie Piccand,[1,9] Filippo De Franceschi,[2] Yuki Ohi,[3] Anindita Bhoumik,[3] Christophe Boss,[4] Umberto De Marchi,[5] Guillaume Jacot,[6] Sylviane Metairon,[7] Patrick Descombes,[7] Andreas Wiederkehr,[5] Alessio Palini,[2] Nicolas Bouche,[4] Pascal Steiner,[8] Olivia G. Kelly,[3] and Marine R.-C. Kraus[1,*]

[1]Nestlé Research, Nestlé Institute of Health Sciences, Stem Cells Unit, EPFL Innovation Park, Building G, 1015 Lausanne, Switzerland
[2]Nestlé Research, Nestlé Institute of Health Sciences, Department of Flow Cytometry, Lausanne, Switzerland
[3]ViaCyte, San Diego, CA, USA
[4]Nestlé Research, Nestlé Institute of Health Sciences, Department of Device Engineering, Lausanne, Switzerland
[5]Nestlé Research, Nestlé Institute of Health Sciences, Department of Mitochondrial Function, Lausanne, Switzerland
[6]Nestlé Research, Nestlé Institute of Health Sciences, Department of Natural Bioactive and Screening, Lausanne, Switzerland
[7]Nestlé Research, Nestlé Institute of Health Sciences, Department of Functional Genomics, Lausanne, Switzerland
[8]Nestlé Research, Nestlé Institute of Health Sciences, Department of Brain Health, Lausanne, Switzerland
[9]Co-first author
*Correspondence: marine.kraus@rd.nestle.com
https://doi.org/10.1016/j.stemcr.2019.02.002

SUMMARY

In type 1 diabetes, a renewable source of human pancreatic β cells, in particular from human induced pluripotent stem cell (hiPSC) origin, would greatly benefit cell therapy. Earlier work showed that pancreatic progenitors differentiated from human embryonic stem cells *in vitro* can further mature to become glucose responsive following macroencapsulation and transplantation in mice. Here we took a similar approach optimizing the generation of pancreatic progenitors from hiPSCs. This work demonstrates that hiPSCs differentiated to pancreatic endoderm *in vitro* can be efficiently and robustly generated under large-scale conditions. The hiPSC-derived pancreatic endoderm cells (HiPECs) can further differentiate into glucose-responsive islet-like cells following macroencapsulation and *in vivo* implantation. The HiPECs can protect mice from streptozotocin-induced hyperglycemia and maintain normal glucose homeostasis and equilibrated plasma glucose concentrations at levels similar to the human set point. These results further validate the potential use of hiPSC-derived islet cells for application in clinical settings.

INTRODUCTION

Diabetes currently affects about 400 million people worldwide, of which type 1 diabetes (T1D) accounts for up to 5%–10%. Indeed, T1D was recognized early in the era of regenerative medicine research as an indication for a stem cell-based therapy as it results from the lack of insulin due the loss of pancreatic β cells. In these patients blood glucose homeostasis must be controlled through the injection of insulin. An alternative approach is the transplantation of islets or β cell preparations obtained post-mortem from organ donors. Although success rates have increased, the duration of insulin independence following transplantation is usually restricted to a few years (Shapiro et al., 2000). The rate-limiting step for the widespread use of islet cell transplantation is a reproducible unlimited supply of functional beta/islet cells. Regenerative medicine approaches therefore represent an important possibility for achieving this breakthrough. Over the last decade, significant advancements have been made to develop alternative β cell replacement therapies using a renewable source of differentiating cells such as human pluripotent stem cells. Endoderm patterning principles have been mimicked *in vitro* to differentiate human embryonic stem cells (hESCs) or human induced pluripotent stem cells (hiPSCs)

into pancreatic endoderm cells (PECs) that express the transcription factors NKX6-1 and PDX1 (D'Amour et al., 2006; Nostro et al., 2011; Nostro et al., 2015). *In vivo* implantation of such ESC-derived PECs led to further differentiation and maturation into insulin-producing cells, culminating in the first clinical trial using stem cell therapy for T1D (ViaCyte, Inc., clinical trials identifier: NCT02239354) (D'Amour et al., 2006; Jiang et al., 2007; Kroon et al., 2008; Zhang et al., 2009; Kelly et al., 2011; Rezania et al., 2012). The recent discovery that it is possible to derive hiPSCs from somatic cells has raised the possibility that β cells can be derived from patients themselves through cell reprogramming and differentiation. While the use of pluripotent stem cells is the most promising strategy for cell replacement therapy, it may not prevent the need for immunosuppressant drugs in the context of T1D with islet-specific autoantibodies. Although improvements of immunosuppression protocols have been made, they are still associated with impaired β cell regeneration and function (Dominguez-Bendala et al., 2016; Shapiro, 2011). Recently, a macroencapsulation device has been put forward as a means to protect β cells from host immunoreactivity (Kumagai-Braesch et al., 2013). Macroencapsulation devices are cell-impermeable porous membrane cassettes employed to encase and immunoprotect the

engrafted cells. It has been shown that macroencapsulation and more recently microencapsulation of hESC-derived pancreatic progenitors differentiated into β cells could partially rescue streptozotocin (STZ)-induced hyperglycemia without triggering an immune response (Kroon et al., 2008; Lee et al., 2009; Robert et al., 2018; Vegas et al., 2016). In the present study we assessed the potential of hiPSCs to efficiently differentiate into pancreatic progenitors in a scalable and reproducible process. Further, we investigated the capacity of the hiPSC-derived pancreatic progenitor cells to survive and mature within planar macroencapsulation devices *in vivo* to levels allowing prevention of hyperglycemia in animals after ablation of mouse β cells using STZ.

RESULTS

In Vitro Characterization of hiPSC Differentiation into Pancreatic Endoderm Cells

hiPSCs were differentiated into PECs using an optimized version of a four-stage protocol published previously (D'Amour et al., 2005; D'Amour et al., 2006; Kroon et al., 2008). Two hiPSC lines derived from different donors were initially cultured as monolayers and controlled for pluripotency by flow cytometry (data not shown) before initiating 12 days of differentiation under three-dimensional culture conditions. Quantitative gene expression analysis revealed specific patterns recapitulating the different stages of differentiation in normal endocrine development and showed consistency between the two hiPSC lines (Figures 1A–1I). During the first 2 days of differentiation, induction of endoderm fate occurs. hiPSCs lose the expression of pluripotency markers (*NANOG*, *POU5F1*, and *SOX2*) and start expressing the mesoendodermal stage-specific marker *T-box transcription factor T* (*TBXT*) and then the definitive endoderm-specific markers *SOX17* and *CXCR4* (Figures 1A–1F). This stage is followed by specification of primitive gut tube together with upregulation of *HNF1B* and *HNF4A* (data not shown) at day 5 before expressing markers of posterior foregut as indicated by increased expression of *SOX9* and *PDX1* at day 8 of differentiation (Figures 1G and 1H). By day 12, *NKX6-1* gene expression levels are dramatically increased (Figure 1I), indicating the beginning of pancreatic endocrine specification. At this time point, a large proportion of endodermal chromogranin A-negative/PDX1-positive cells also express NKX6-1 (49.03% ± 6.1%) as shown by immunofluorescence and flow cytometry analyses (Figures 1J, 2A, 2B, and 2D). These cells are considered pancreatic endocrine progenitors and will be referred to as PECs throughout, while the aggregates will be named hiPSC-derived PECs (HiPECs). A small proportion of cells

express CDX2 and/or AFP (14.06% ± 1.8%) and likely represent off-target gut endoderm cells (Figures 2C and 2D). Moreover, a small percentage of differentiating chromogranin A-positive cells (total endocrine, Figures 2A and 2D, 19.77% ± 4.7%) is detected, which mainly represents cells co-expressing insulin and glucagon (Figure 1K) or insulin and somatostatin (not shown). Similar cell populations have been identified in PECs derived from hESCs (Robert et al., 2018). The four-stage differentiation protocol of hiPSCs into pancreatic endocrine progenitors described here was further adapted to large-scale culture conditions following a previously published protocol using hESCs (Schulz, 2015; Schulz et al., 2012). Typically, large-scale production was initiated from 3–7 * 10^9 hiPSCs in 30,000–40,000 cm². The timing of gene expression of small- versus large-scale culture similarly recapitulated the four-stage differentiation process (data not shown). In large-scale aggregates (herein named LHiPECs), the percentage of PECs was comparable at day 12 to small-scale generated HiPECs (HiPECs, 49.03% ± 6.1%; LHiPECs, 46.22% ± 3.04%) (Figures 2D–2F). Moreover, LHiPECs could be frozen and stored without losing their differentiation status as shown by flow cytometry analyses of LHiPECs after cryopreservation and thawing (Figures 2G and 2H). Taken together, these results show that the four-stage differentiation protocol allows the differentiation of hiPSCs into pancreatic endoderm expressing the appropriate sets of genes and proteins consistent with this stage of differentiation. Moreover, these data demonstrate that the method is reproducible, robust, and scalable for production of large batches of PECs of high quality that can be cryopreserved prior to further use.

Macroencapsulated hiPSC-Derived Pancreatic Endoderm Generates Functional Endocrine Cells *In Vivo*

To investigate whether *in vitro*-produced HiPECs have the potential to generate functional endocrine cells *in vivo*, we used a flat-sheet macroencapsulation device to graft the HiPECs under the skin (neck) of immune-compromised mice (Lathuiliere et al., 2014). We initially determined and set the optimal volume of cells to engraft at 45 μL (4–5 * 10^6 cells) of aggregates (Figure S1). Starting at 8 weeks post-implantation, we investigated the efficiency of β cell differentiation *in vivo* by analyzing changes in serum human c-peptide release during glucose challenges (Figures 3A and 3A'). At 8 weeks post-implantation, very low levels of human c-peptide (<100 pM at 60 min) were detected in response to glucose administration (Figure 3A). Four weeks later, an increase in c-peptide levels was observed (315.1 ± 19.92 pM) 60 min after glucose administration. With increasing number of weeks *in vivo*, both fasting and glucose-stimulated human c-peptide levels continued
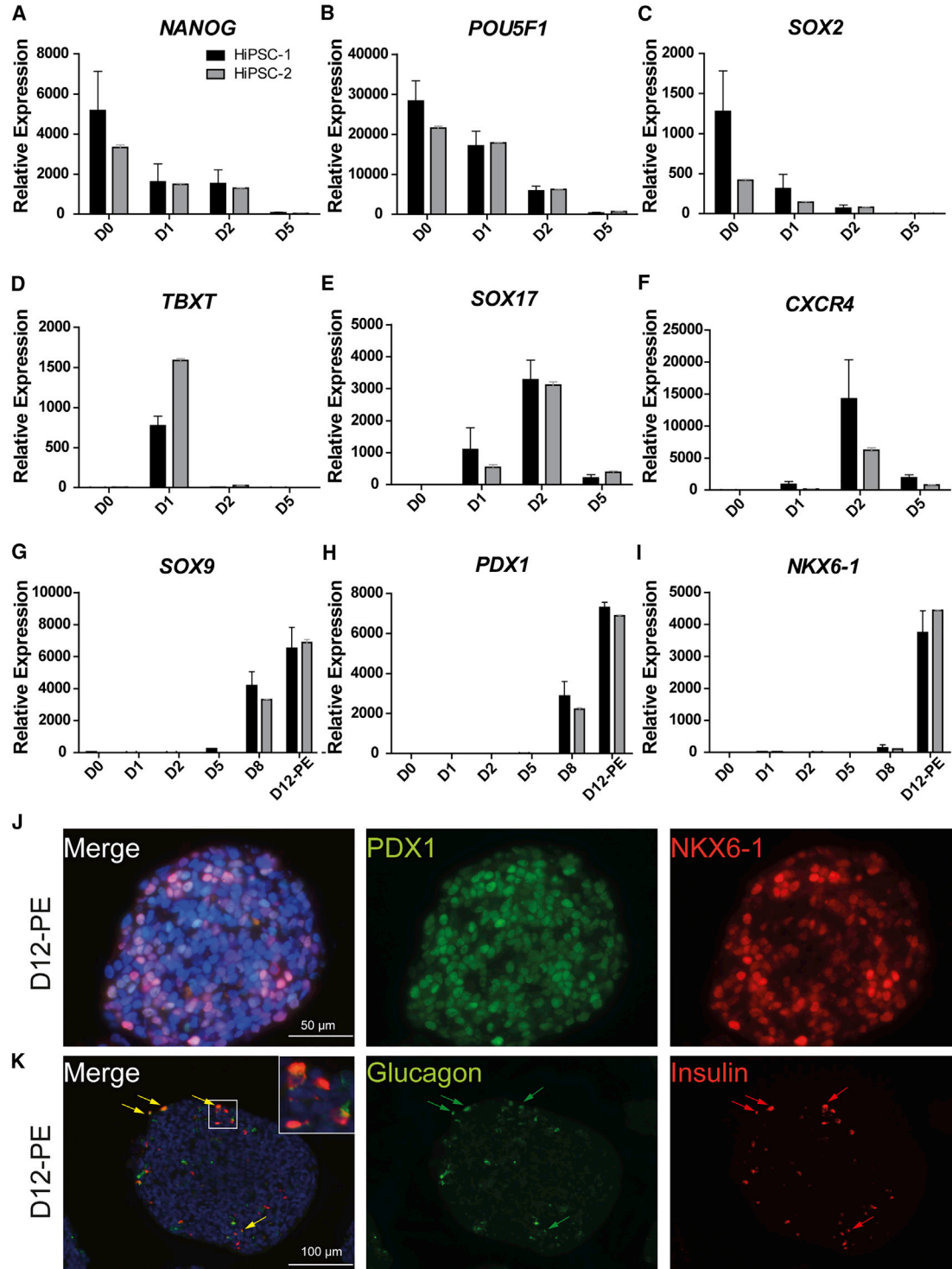
Figure 1. Characterization of hiPSC Differentiation toward Pancreatic Endoderm Cells

(A–I) RNA expression analyses of important markers modulated during differentiation of hiPSCs toward pancreatic endoderm stage comparing two different hiPSC lines, HiPSC-1 and HiPSC-2 (n = 3 independent experiments with technical duplicates). (A) *NANOG*, (B) *POU5F1*, (C) *SOX2*, (D) *T*, (E) *SOX17*, (F) *CXCR4*, (G) *SOX9*, (H) *PDX1*, (I) *NKX6.1*. Chart bars represent relative expression value average and error bars represent SD. (J and K) Immunofluorescence of cell aggregates at pancreatic endoderm stage (D12-PE). (J) Staining for PDX1 and NKX6-1. Scale bar, 50 μm. (K) Staining for glucagon and insulin. Scale bar, 100 μm. Arrows show polyhormonal cells. Nuclei are stained in blue with DAPI.
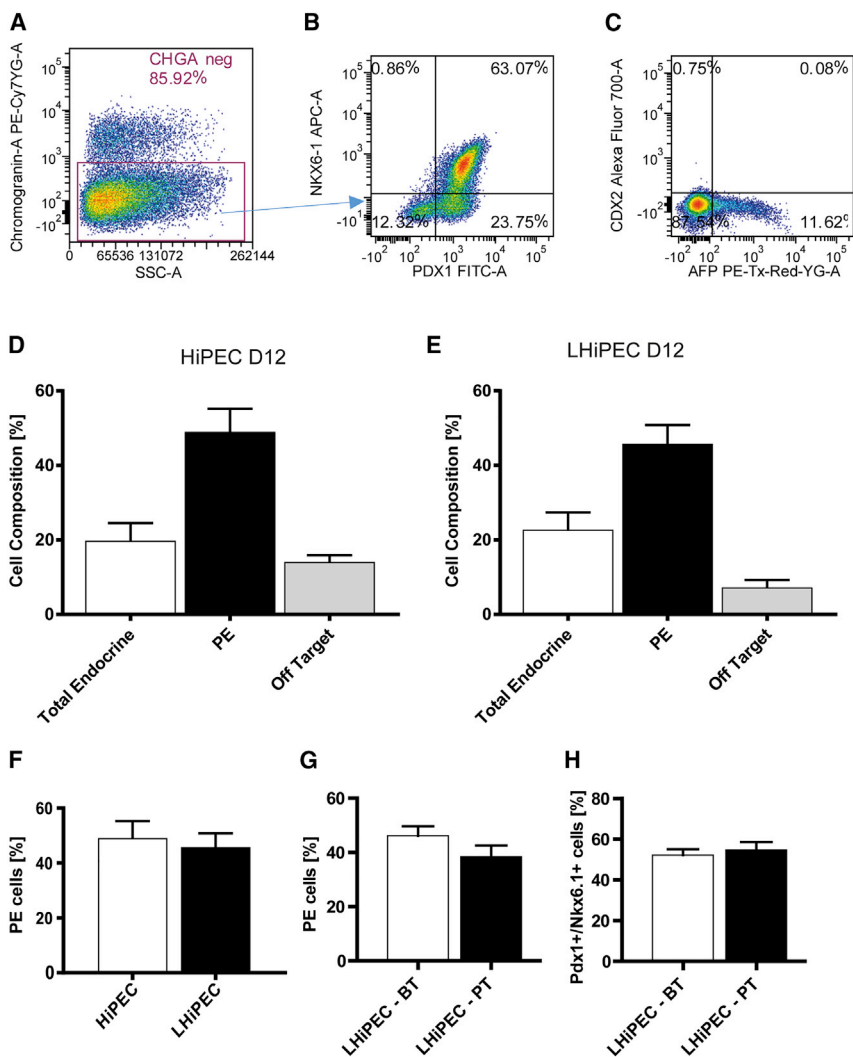
Figure 2. Cell Composition Analyses of Hi-PECs and LHiPECs

(A–C) Flow cytometry analysis of cell composition of HiPEC and LHiPEC at day 12 of differentiation. Cells were labeled to determine the endocrine polyhormonal population (chromogranin A positive), the pancreatic endoderm population (chromogranin A negative, PDX1$^+$ and NKX6-1$^+$), and the off-target population (CDX2$^+$, AFP$^+$). Representative pictures from flow cytometry analysis of (A) chromogranin A (gated on side scatter), (B) PDX1 and NKX6-1 (gated on chromogranin A negative), and (C) AFP and CDX2 (gated on side scatter).

(D and E) Ratios over the total population for each individual population of (D) HiPEC and (E) LHiPEC generated cells.

(F) Comparison of percentage of PECs in HiPECs versus LHiPECs.

(G) Comparison of percentage of PECs in LHiPECs before and after cryopreservation.

(H) Comparison of percentage of PDX1$^+$/NKX6-1$^+$ cells in LHiPECs before and after cryopreservation. For HiPEC and LHiPEC analyses, n = 5 and n = 8 independent experiments, respectively. Error bars represent SEM.

to rise to reach a maximum of 292 ± 34.63 pM at fasting and 1,203 ± 178 pM at 60 min peak levels in response to glucose after 18 weeks post-implantation (Figure 3A). These results were consistent with encapsulated cells derived from different parental hiPSC lines (Figure 3C). Moreover, similar results were observed in mice implanted with LHiPECs (Figure 3A′), although serum human c-peptide levels were lower in magnitude compared with the corresponding values obtained from HiPECs. Independent of the cell source, glucose-induced secretion and kinetics of c-peptide release were similar (Figure 3A′). When tested after shorter periods of time *in vivo*, c-peptide secretion was maximal at 60 min post-glucose injection (12 and 16 weeks post-implantation). Peak c-peptide release shifted to 30 min post-glucose when animals were assessed at later times after implantation (>18 weeks). These results suggest that the maturation of HiPEC-derived β cells continues over time *in vivo*.

To further characterize the role of HiPEC-derived endocrine cells in the regulation of glucose metabolism *in vivo*, we compared the serum levels of human c-peptide and glucose clearance over time. In this analysis both mouse islet β cells and implanted human β cells contributed to lower blood glucose levels during the tolerance test. As human insulin secretion measured by c-peptide analysis increased with time following implantation, this may exaggerate the corrective action of insulin on glucose homeostasis. Indeed, after 20 to 22 weeks of implantation of either HiPECs or LHiPECs, glucose clearance was significantly accelerated compared with animals carrying the macroencapsulated cells for only 8 weeks (Figures 3B and 3B′). Enhanced correction of glucose excursions occurred over the same time frame as graft-derived human c-peptide increased (Figures 3A, 3B, 3A′, and 3B′). In parallel, fasting blood glucose levels decreased (from 99.06 ± 3.2 mg/dL at 8–9 weeks post-implantation to 87.67 ± 4.3 mg/dL at 20 weeks)
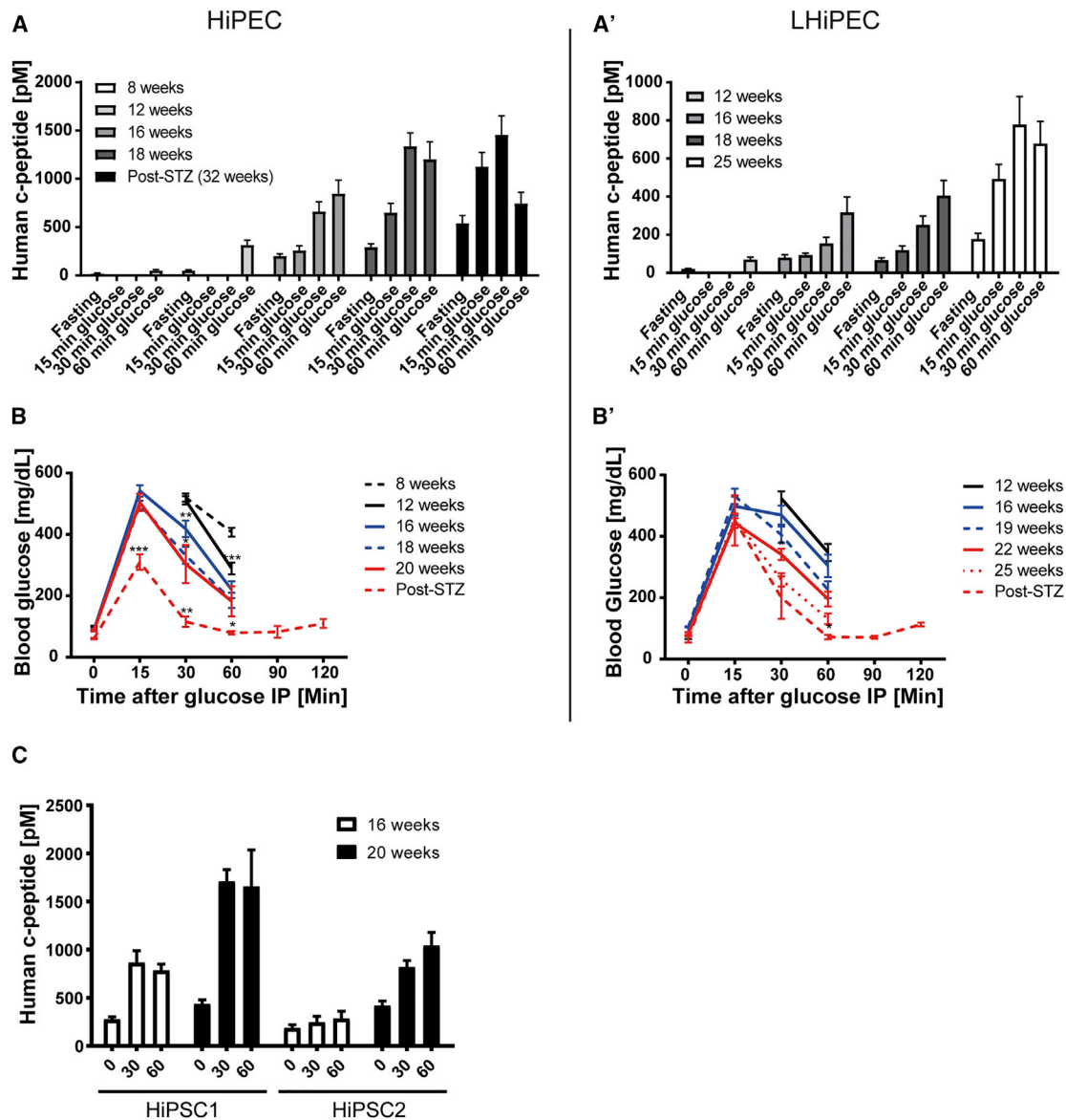
Figure 3. Human c-peptide Detected in Sera of Mice Implanted with HiPECs and LHiPECs

(A and A') Analyses of blood glucose levels and serum levels of human c-peptide in mice implanted with hiPSC-derived pancreatic endoderm cells. Mice implanted with (A) HiPSC-1-derived or (A') LHiPSC-derived pancreatic endoderm cells were analyzed at the corresponding indicated post-engraftment times for serum levels of human c-peptide following intraperitoneal glucose administration.

(B and B') (B) Mice implanted with cells as shown in (A), and (B') those shown in (A'), were analyzed at the indicated post-engraftment times for blood glucose levels following intraperitoneal (IP) glucose administration. Averages of blood glucose levels in response to intraperitoneal glucose tolerance test are shown for the indicated post-engraftment times. (A and B) n = 20–29 animals (three independent experiments); (A' and B') n = 12 animals (two independent experiments).

(C) Comparative analyses at the indicated post-engraftment times of serum levels of human c-peptide in cohorts of mice implanted with HiPSC-1-derived pancreatic endoderm cells (n = 9 animals, two independent experiments) or HiPSC-2-derived pancreatic endoderm cells (n = 5 animals). Error bars indicate SEM.

Statistical analysis was performed by Student's t test (*p < 0.05; **p < 0.01; ***p < 0.001).

(Figure 3B). Similar changes in fasting blood glucose levels were observed in animals implanted with LHiPECs (Figure 3B'). Altogether these data strongly suggest that insulin release from implanted hiPSC-derived PECs is under glucose control and significantly contributes to glucose homeostasis in the host.
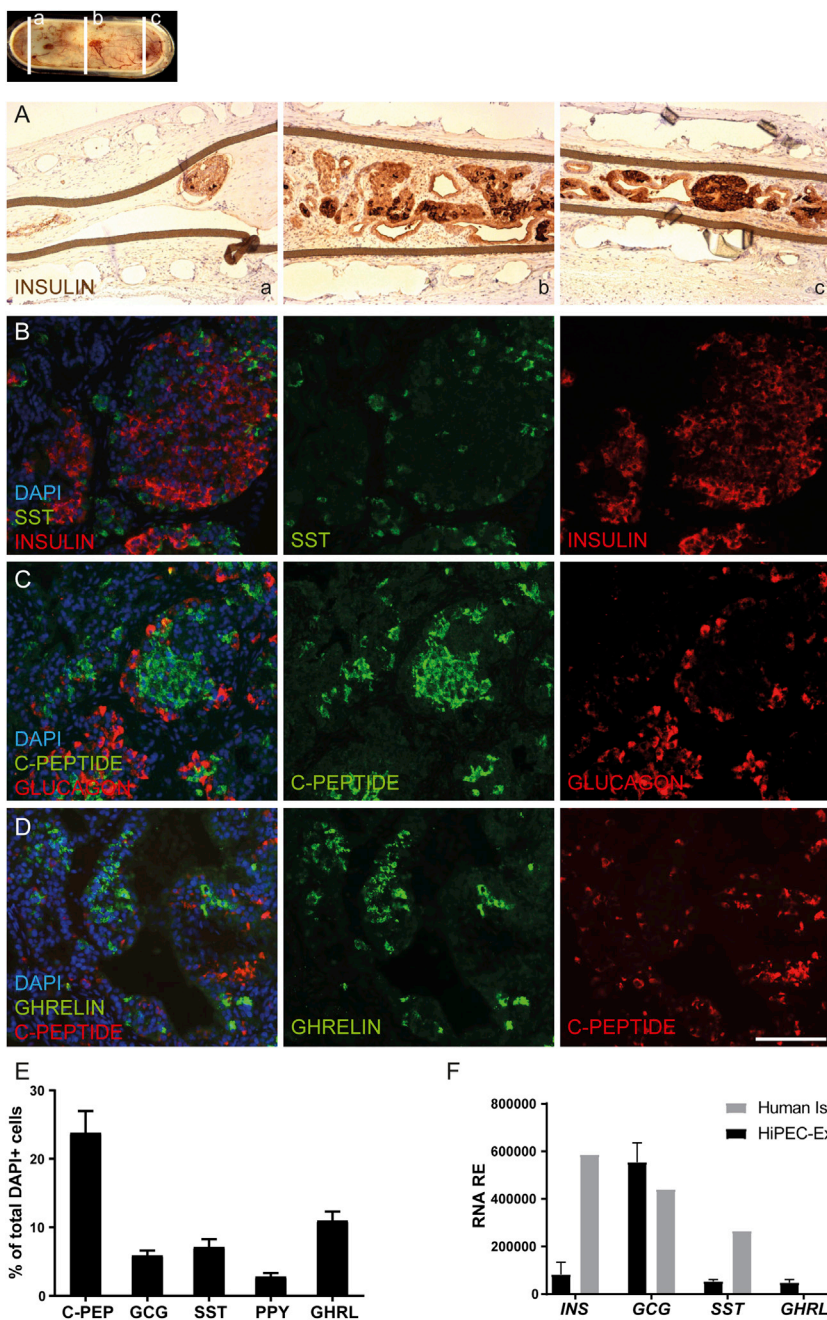
Figure 4. Pancreatic Endocrine Hormone Expression in HiPEC-1-Derived Grafts

Micrographs of serial sections of immuno-histochemistry and immunofluorescence analyses of HiPEC-1-derived graft samples 32 weeks post-engraftment for pancreatic endocrine hormone expression.

(A) Staining for insulin.

(B) Staining for somatostatin (SST) and insulin.

(C) Staining for human c-peptide and glucagon.

(D) Staining for ghrelin and c-peptide. Scale bar, 100 μm.

(E) Cell composition quantification by high content image analysis of the indicated pancreatic endocrine hormones. Values were normalized to DAPI-positive cells (n = 6 explants).

(F) RNA expression analysis of the indicated markers in HiPEC-1-derived explants (n = 2 explants) and control human islet (n = 2 donors) samples. Error bars indicate SD.

Ex Vivo Characterization of HiPEC-Derived Glucose-Responsive Insulin-Producing Cells

To characterize the cellular content of the devices, we performed immunohistochemical analyses of explanted grafts 32 weeks post-implantation. The H&E staining of sectioned devices revealed the homogeneous formation and distribution of a three-dimensional, organized tissue derived from HiPECs, while conjunctive tissue (c) as well as vessels (dotted lines) was detected on the outer surface of the device but not in direct contact with cells present inside (Figure S2). We clearly identified epithelial endocrine tissue (straight lines), as well as ductal structures (d) surrounded by connective tissue (*) (Figure S2). Also, insulin staining revealed a high proportion of cells expressing insulin in islet-like structures and a wide distribution of insulin-positive cells throughout the device (Figures 4A and S2). Subsequent immunofluorescence labeling for endocrine hormones, i.e., insulin, glucagon, somatostatin, and ghrelin, showed that typical grafts contained multiple cell clusters individually expressing each hormone in a
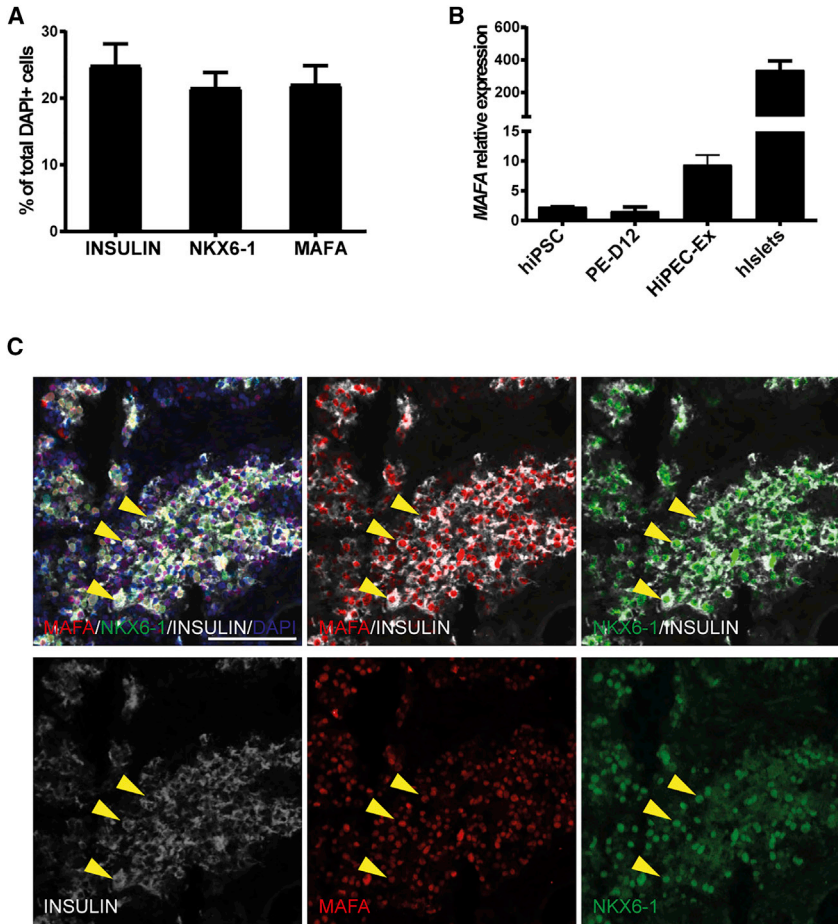
Figure 5. Expression of Mature β Cell Markers in HiPEC-1-Derived Grafts

(A) Cell composition quantification by high content image analysis for insulin, NKX6-1, and MAFA. Values were normalized to DAPI-positive cells (n = 6 animals).

(B) qRT-PCR analyses for *MAFA* transcript in hiPSCs (n = 2 lines), PE-D12 (n = 6 differentiations), explants (n = 4), and human islets (n = 2 donors). Error bars indicate SEM.

(C) Extracted immunofluorescence staining from high content imaging for MAFA (red), NKX6-1 (green), and INSULIN (white). The three yellow arrowheads point to three cells showing triple-positive staining. Scale bar, 50 μm.

heterogeneous cellular architecture reminiscent of either fetal or more mature pancreatic islets (Figures 4B–4D). A small proportion of glucagon cells also expressed c-peptide, representing rare polyhormonal cells present in the explants (Figure 4C). Apart from the endocrine population, we also observed ductal (Figures S2, S3A, and S3B) and mesenchymal cells (Figure S3C), which express CK19 and vimentin, respectively. However, we did not detect positive cells for CDX2, albumin, and amylase (data not shown). This is in agreement with the absence of exocrine, intestinal, and hepatic transcripts in explanted grafts (Figures S3D and S3F). Moreover, we did not detect remaining pluripotent cells or teratoma formation in the explants (Figure S3G and data not shown). Accordingly, in a recent longitudinal proteomic profiling study (Haller et al., 2018) of PEC differentiation *in vivo*, we could not detect any protein corresponding to those off-target tissues after 16 weeks of implantation.

HiPEC-derived tissue contained more than 50% endocrine cells, with 23.79% ± 3.19% c-peptide positive, 5.88% ± 0.73% glucagon positive, 7.15% ± 1.11% somatostatin positive, 2.79% ± 0.54% pancreatic polypeptide pos-

itive, and 11.00% ± 1.32% expressing ghrelin (Figure 4E). Similar to the proportion of c-peptide-positive cells, 24.86% ± 3.28% of total cells expressed insulin, which suggests that more than 95% of insulin cells also express c-peptide (Figures 4E and 5A and data not shown). Gene expression analysis of the grafts confirmed the presence of *insulin*, *glucagon*, *somatostatin*, and *ghrelin* as well as *MAFA* and *NKX6.1* transcripts (Figures 4F, 5B, S4, S5A, and S5B). Indeed, MAFA and NKX6.1 are two important transcription factors involved in the function and the maintenance of the glucose-responsive phenotype of mature β cells (Matsuoka et al., 2004; Zhang et al., 2005). Compared with human islets obtained from adult post-mortem donors, *insulin* and *somatostatin* expression was lower in the grafts (Figure 4F). This can be explained by the dilution of the endocrine population in the explant grafts compared with control human islet preparations. However, *glucagon* and *ghrelin* were expressed at slightly higher levels than those measured in human islets, which could suggest a bias in the differentiation potential or the prevalence of a progenitor state. We could quantify similar percentages of cells positive for insulin (24.86% ± 3.28%; n = 6), NKX6-1
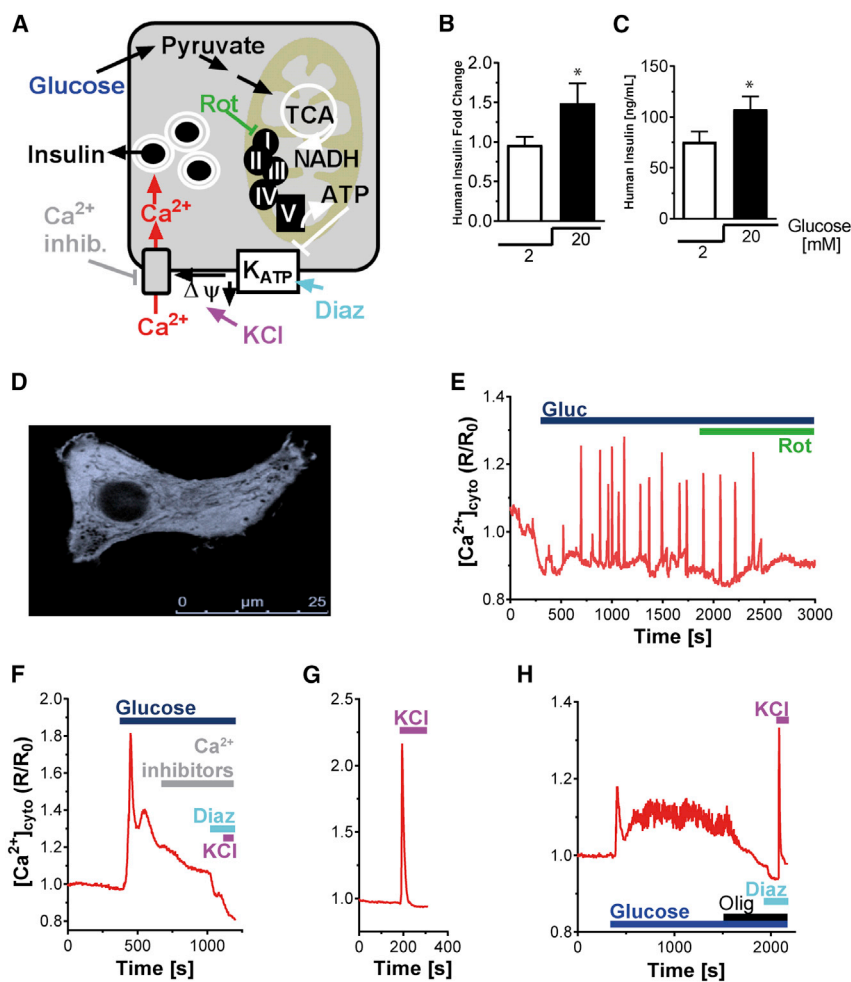
Figure 6. Glucose-Stimulated Ca²⁺-Signaling Pathway Characterization in hiPSC-Derived Pancreatic β Cells after *In Vivo* Differentiation

(A) Model for Ca^{2+}-dependent coupling of glucose metabolism to insulin secretion in the pancreatic β cells.

(B and C) Human insulin secretion levels measured on *ex vivo* tissue samples after glucose exposure. Values are expressed as (B) fold change (n = 8 explants; *p = 0.0371) or (C) concentration (ng/mL) (*p = 0.0352) (C).

(D) Cytosolic signal of Ca^{2+} sensor AD-RIP-YC3.6cyto recorded at 535 nm in HiPEC-1-derived β cells. Scale bar, 25 μm.

(E–G) Examples of Ca^{2+} responses in individual HiPEC-1-derived β cells, stimulated with 16.7 mM glucose and subsequently treated with (E) Rotenone (Rot; 1 μM), (F) diazoxide (Diaz; 100 μM; K_{ATP} channel activator), and the three voltage-dependent Ca^{2+} channel blockers (Ca^{2+} inhibitor: Isidipine [20 μM], ω-agatoxin [400 nM], NNC 55-0396 [2 μM]) (F), and KCl (30 mM) (F and G). The ratiometric signals were normalized to basal (set to 1). Data are representative of 14 glucose stimulation experiments (40 cells). Diazoxide, Rotenone, and KCl effects were confirmed in 11, 6, and 7 experiments, respectively. The effect of the Ca^{2+}-channels blockers followed by KCl depolarization was repeated three times.

(H) Example of a control human β cell Ca^{2+} signaling trace. Statistical analysis was performed by Student's t test. Error bars indicate SEM.

(21.52% ± 2.31%), and MAFA (22.02% ± 2.86%) (Figure 5A). Co-localization analysis also showed that the majority of the insulin-positive cells were positive for NKX6-1 and/or MAFA (Figure 5C). These different hormones and transcription factors are hallmarks of fully differentiated pancreatic endocrine cells and emphasize the fact that a reasonable fraction of HiPEC-derived endocrine cells have reached a mature phenotype.

Metabolism-Secretion Coupling in HiPEC-Derived Insulin-Producing Cells

β cell metabolism-secretion coupling is a multistep process linking glucose metabolism to insulin secretion. Glucose metabolism results in mitochondrial activation and enhanced ATP formation. The elevated cytosolic ATP/ADP ratio favors closure of K_{ATP} channels leading to plasma membrane depolarization. Voltage-gated Ca^{2+} influx finally triggers insulin secretion (Figure 6A). To determine whether the HiPEC-derived insulin-secreting cells differentiated

in vivo were capable of responding to glucose, we characterized glucose-dependent insulin secretion. After 25 weeks *in vivo*, devices were explanted and tested *ex vivo* for static glucose-stimulated insulin secretion. Glucose significantly increased insulin secretion by 1.48 ± 0.25-fold compared with grafts maintained under resting glucose conditions (Figures 6B and 6C). As a second measure of β cell activation we measured Ca^{2+} response in HiPEC-derived endocrine cells. We performed single-cell fluorescence-based identification of insulin-expressing cells in graft tissue infected with adenovirus expressing the cytosolic Ca^{2+} sensor YC3.6cyto (AD-RIPYC3.6cyto) (Figure 6D). HiPEC-derived insulin-positive cells exhibited a Ca^{2+} response following 16.7 mM glucose stimulation (Figures 6E and 6F). The glucose-dependent Ca^{2+} increases were heterogeneous, showing both oscillatory and biphasic kinetics (Figures 6E and 6F), comparable to recordings of adult human primary β cells (Figure 6H) previously reported by others (De Marchi et al., 2014). Direct plasma membrane depolarization
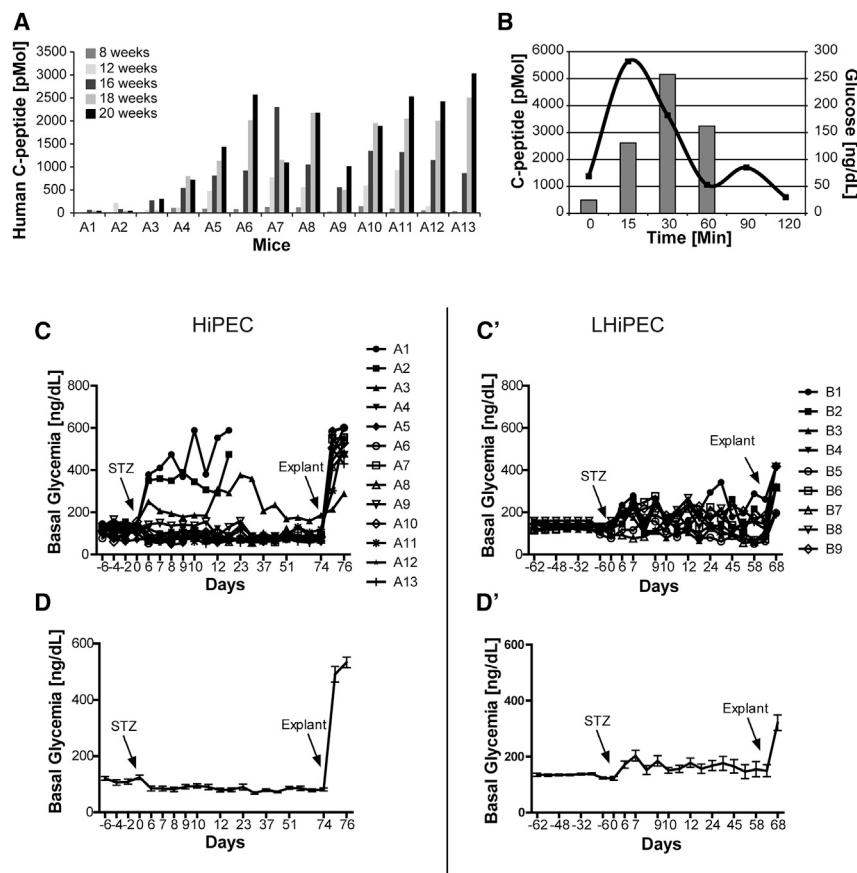
Figure 7. Analyses of STZ-Treated Mice

(A) Mice implanted with HiPECs were analyzed at the indicated weeks post-engraftment for serum levels of human c-peptide after intraperitoneal glucose administration. The highest c-peptide values detected post-glucose challenge are represented for each time point.

(B) Glucose tolerance test, blood glucose levels, and c-peptide levels are shown for mouse A5 after intraperitoneal glucose administration.

(C, C′, D, and D′) (C) Independent and (D) average values of non-fasting blood glucose levels measured in 13 animals represented in (A) before and for 74 days after STZ treatment (STZ at 22 weeks post-engraftment time). Average values exclude animals A1, A2, and A3 that lost glucose control due to the absence of human c-peptide secretion. At day 74 post-STZ (10 weeks), mice were explanted and blood glucose levels were monitored post-explantation. (C′) Independent and (D′) average values of non-fasting blood glucose levels measured before and for 68 days after STZ treatment (STZ at 25 weeks post-engraftment time) in 9 animals implanted with LHiPECs. At day 67 post-STZ (9 weeks), mice were explanted and blood glucose levels were measured post-explantation. Error bars represent SEM.

applying a final concentration of 30 mM KCl caused an immediate and transient Ca^{2+} rise in HiPEC-derived β cells, indicating the presence of functional voltage-gated Ca^{2+} channels and normal Ca^{2+} efflux mechanisms (Figure 6G). As in human β cells, inhibition of mitochondrial respiration using rotenone (Figures 6E and 6H) or blockage of the voltage-dependent Ca^{2+} channels (Figure 6F) prevented cytosolic Ca^{2+} increases. Taken together, these results demonstrate that metabolism-secretion coupling in HiPEC-derived β cells relies on mitochondrial function, plasma membrane depolarization, and voltage-dependent Ca^{2+} influx, comparable to primary β cells.

Macroencapsulated HiPEC-Derived Endocrine Cells Protect Mice against STZ-Induced Hyperglycemia

The ultimate test to validate the functionality of HiPEC-derived endocrine cells is to assess their ability to regulate blood glucose levels independent of the endogenous mouse pancreatic β cells. We showed earlier that macroencapsulated HiPEC-derived β cells improved glucose clearance after glucose challenge over time. To further investigate the ability of grafted cells to tightly regulate glucose levels, engrafted mice were treated with the β cell toxin

STZ. To exert its toxic function, STZ enters β cells through the glucose transporter SLC2A2 (GLUT2). Human β cells express relatively low levels of SLC2A2 and are therefore protected from STZ cytotoxicity at doses that eliminate mouse β cells (Yang and Wright, 2002). As expected, animals with levels of circulating human c-peptide below 100 pM (animals A1 and A2) became hyperglycemic after STZ treatment, showing the efficiency of the murine β cell depletion (Figures 7A and 7C). In contrast, animals with circulating human c-peptide levels over 500 pM maintained normoglycemia (Figures 7A–7C). Indeed, murine c-peptide levels induced by a glucose challenge in mice are normally around 500–600 pM at peak, which suggests that this level of human c-peptide is adequate to improve glucose control. Also, when comparing the profiles of human c-peptide secretion after glucose injection before and after STZ treatment, we observed that the engrafted cells maintained their function at maximal values, with the highest peak of secretion after 30 min (Figure 3A). This observation was independent of the cell source used for the implantation (HiPEC versus LHiPEC).

Interestingly, glucose clearance efficiency was significantly improved in animals after STZ treatment compared

with the same animals before STZ treatment. Indeed, blood sugar rise after glucose challenge was significantly lower and returned to baseline more rapidly (Figures 3B, 3B′, and 7B). These results suggest that engrafted cells further mature with time and/or when full contribution is needed. As demonstrated, basal blood glucose levels of animals post-STZ remained tightly controlled for several weeks after treatment (Figures 7C and 7D). The control of glycemia in animals implanted with LHiPECs was more unstable following STZ and we could observe a moderate delay before stabilization of basal blood glucose levels, reflecting slightly lower and delayed levels of circulating human c-peptide in these cohorts (Figures 7C′ and 7D′).

After murine β cell ablation, basal blood glucose concentration was initially between 105 and 125 mg/dL but by 1–2 weeks stabilized lower at 70 to 90 mg/dL (Figure 7D). These concentrations are in the range of the reported human set point of 70–120 mg/dL. Resetting of basal blood glucose concentration also occurred in animals implanted with LHiPECs to some extent, but due to the delay in maturation it was less robust on average (Figure 7D′). Removal of the implants rendered animals strongly hyperglycemic (500–600 mg/dL glucose) (Figures 7D and 7D′). These data support several conclusions. First, graft-derived endocrine cells are capable of maintaining glucose homeostasis in the absence of mouse pancreatic β cells (Figure S6). Second, rising serum levels of graft-derived insulin as observed over time resulted in a gradual decrease of blood glucose concentrations. Finally, prevention of hyperglycemia in SCID/Bg mice whose endogenous β cells had been destroyed required human graft-derived glucose-stimulated serum levels of human c-peptide of 500 pM (2.3 ng/mL) or more.

DISCUSSION

In this study, we examined the potential of hiPSCs to differentiate into pancreatic progenitors using a four-stage protocol originally developed for hESCs in a scalable process. Our results show that we could reproducibly and efficiently differentiate hiPSCs into PECs applying both a small- and a large-scale protocol. PECs were qualified by negative expression of CHGA and high levels of expression of PDX1 and NKX6-1 as well as FOXA2. The differentiation efficiency was in a range similar to that previously observed by others for hiPSCs (Nostro et al., 2015). However, accurate comparison is difficult as there is no consensus on the methods used to quantify the percentage of PECs. Although we did observe a small proportion of mostly polyhormonal endocrine cells as well as cells expressing off-target markers such as intestinal (CDX2) and liver (AFP) markers, we speculate that the glucose-responsive cells arise from pancreatic endoderm-defined cells. This is based on prior work performed on hESC-derived PECs showing that insulin-producing cells generated in vivo derive from sorted PECs, whereas the polyhormonal cells give rise to mainly glucagon cells (Kelly et al., 2011). Also, others have shown that differentiated populations containing higher proportions of pancreatic progenitor cells expressing PDX1 and NKX6-1 differentiate toward β-like cells either in vivo or in vitro (Kirk et al., 2014; Pagliuca et al., 2014; Rezania et al., 2014; Russ et al., 2015). Using more recently published protocols with the large-scale three-dimensional system described here, it is likely that the four-stage differentiation protocol could be further optimized to increase the percentage of PECs and decrease the percentage of polyhormonal endocrine cells. This study represents a valid proof of concept that hiPSC-derived pancreatic endoderm can be generated in large-scale production.

The capacity of hiPSC-derived PECs to survive and mature within planar macroencapsulation devices in vivo was evaluated. Explants of hiPSC-derived β cells in the context of other islet cells generated in vivo secrete human insulin and c-peptide in response to glucose. Furthermore, glucose triggered calcium signaling in the β cells matured in vivo, consistent with normal metabolism-secretion coupling in these cells. Importantly, following more than 12 weeks of implantation, the hiPSC-derived PECs were able to prevent hyperglycemia in 70%–80% of animals after ablation of mouse β cells using STZ. The minimal requirement for STZ-driven hyperglycemia protection in mice was around 500 pM release of human c-peptide, which corresponds to reported maximal concentrations of murine c-peptide secreted after glucose injection. However, the range of glucose-stimulated c-peptide levels measured in insulin-free diabetic patients with functional islet grafts averaged 3–4.5 ng/mL (1,000–1,500 pM) (Hering et al., 2005), comparable to the 1,456 ± 300 pM levels detected after STZ ablation. The rescue of the STZ-driven hyperglycemia was as efficient as observed after transplantation of hESC-derived PECs or with approximately 2,000 adult human islets (Gaber et al., 2004; Kroon et al., 2008). In vivo-matured hiPSC-derived PECs tightly controlled glycemia below the levels observed before the STZ ablation, reaching an average of 80 mg/dL for a period of up to 70 days following the STZ treatment. Relative to plasma glucose levels in humans, which are 70–120 mg/dL, the calibrated levels ranged from normoglycemic to slightly hypoglycemic. Hypoglycemia (with respect to normal mouse basal levels) is generally observed in mice and rats upon engraftment of human fetal or adult β cells (Castaing et al., 2001; Tuch et al., 1991), as well as hESC-derived β cells (Kroon et al., 2008). In this study we decided to assess the maturation of hiPSC-derived β cells under

normoglycemic conditions, which do not reflect the clinical conditions of treatment of T1D. However, normoglycemia in mice is perceived as a mild hyperglycemic environment for human PECs with regard to human physiology.

Glucose-stimulated human c-peptide levels were detected in serum around 8 weeks post-implantation for the HiPECs and after 12 weeks for the LHiPECs. In general, large-scale production tended to influence the maturation efficiency of the pancreatic endoderm compared with the small-scale production, an effect that did not appear to be attributable to cryopreservation of PECs (data not shown). The reduction of growth factor concentrations used during the large-scale production to reduce costs may explain the reduced efficiency, although this change did not have an impact on the percentage of PECs obtained at the differentiation endpoint. Notably, some mice implanted with the LHiPECs demonstrated c-peptide kinetics comparable to those of mice implanted with HiPECs, although the proportion of those animals was smaller in the large-scale cohorts. The reason for this difference is unclear; it could be due to variability observed with *in vivo* experiments or perhaps more variable levels of engraftment with large-scale pancreatic endoderm implants. Compared with available data from hESC-derived PEC implantations, or from fetal and adult islet transplantation, the maturation of the hiPSC-derived PECs also seems to be delayed. Interestingly, Robert et al. have shown that the immature features of the hESC-derived β cells *in vivo* improved over time to reach a functionally mature β cell mass after 1 year of engraftment (Robert et al., 2018). Time could also possibly improve maturation of hiPSC-derived β cells, but this hypothesis will need to be tested. The delay could also be explained by the macroencapsulation of the cells (Motte et al., 2014). Indeed, subcutaneous macroencapsulation imposes on the cells a slight delay before full vascularization takes place. We observed that the first blood vessels were established only 10 to 15 days following the implantation. Usually, preferred implantation sites for islets and related cells are the kidney capsule and the epididymal fat pad, which represent highly vascularized sites. As previously reported for hESC-derived β-like cells (Matveyenko et al., 2010), macroencapsulated HiPECs implanted in nude rats showed only poor c-peptide secretion in 10% of the animals after 20 weeks post-implantation and only if the device was permeabilized, which suggests that vascularization efficiency is even more delayed in nude rats compared with SCID/Bg mice and prevents maturation of the pancreatic progenitors (data not shown). However, this is in contrast with results obtained from Bruin et al., where maturation of insulin-secreting cells from hESCs was accelerated after implantation under the kidney capsule of nude rats (Bruin et al., 2015). Indeed, a macroencapsulation approach can trigger a foreign body response to the implant, with recruitment of foreign body giant cells that can affect oxygenation of the device and the implanted cells (Franz et al., 2011). Altogether, these results suggest that tightly controlling vascularization and tissue reaction in macroencapsulated implants is critical for ensuring proper survival and maturation of the cells. Microencapsulation of pancreatic endoderm-derived β-like cells has also been investigated as an alternative requiring accelerated vascularization of the more mature cells (Vegas et al., 2016). However, an important consideration for this approach is maintaining the integrity of the implanted pancreatic aggregates and avoiding the disruption of the maturing cellular architecture, issues that are often associated with microencapsulation of cells for transplantation.

Recently, considerable progress has been made with the optimization of *in vitro* strategies to differentiate hESCs into mature insulin-secreting β cells (Pagliuca et al., 2014; Rezania et al., 2014; Russ et al., 2015). However, these hESC-derived insulin-secreting β cells still have some limitations. For instance, their glucose responsiveness as assessed *in vitro* remains relatively poor compared with primary human islets. Moreover, gene expression profiling showed that the signature of the newly generated β cells still shared features reminiscent of fetal β cells (Pagliuca et al., 2014; Rezania et al., 2014). Indeed, such cells either partially rescued hyperglycemia induced by STZ *in vivo* or rescued hyperglycemia to a similar extent and over the same time frame as PECs, suggesting that their differentiation into fully mature and functional β cells was not complete (Millman et al., 2016). It still remains to be proven if the glucose-responsive β cells in these 12 week grafts derived from the originally implanted insulin cells or the contaminating pancreatic endoderm. Moreover, the efficiency of differentiation remains very low compared with levels obtained for the PECs. All these data suggest that we still need to understand the mechanisms driving the functional maturation of β cells to transfer such knowledge in a dish.

In conclusion, these results show that hiPSC-derived endocrine cells generated after implantation of pancreatic progenitors produced *in vitro* using a scalable process are functionally similar to hESC-derived islets as well as human islets *in vivo*, supporting evidence that hiPSCs may serve as a renewable source of islets for diabetes cell-replacement therapies.

EXPERIMENTAL PROCEDURES

Cell Culture and Differentiation

hiPSCs, provided by Fujifilm Cellular Dynamics (Madison, WI, USA), were maintained on mouse embryonic fibroblast feeder layers (Millipore, PMEF-N). Cell culture was performed in

humidified incubators at 37°C and 8% CO_2. Small- and large-scale expansion and differentiation were carried out under three-dimensional conditions using an optimized version of the four-stage protocol for which details are explained in the Supplemental Experimental Procedures.

Cryopreservation and Banking of HiPECs

LHiPECs (day 12) were resuspended in cryopreservation medium (90% KOSR/10% DMSO/25 mM HEPES), cryopreserved using a controlled-rate freezer (Planer plc Kryo 560-16) using a specific program (Supplemental Experimental Procedures) and banked in liquid nitrogen.

Encapsulation and Implantation

Cell aggregate slurry was transferred in S4 culture medium and loaded into a flat sheet encapsulation device based on a polymeric frame technology as described previously (Supplemental Experimental Procedures) (Lathuiliere et al., 2014). Encapsulation devices were implanted dorsolaterally in male SCID/Beige mice (Charles River) 6–13 weeks of age. All animal experiments were carried out in accordance with the Swiss regulation on animal experimentation and the European Council directive (86/609/EEC) for the care and use of laboratory animals (EXPANIM-SCAV protocol approval VD2569).

STZ Treatment of Mice

At 20–25 weeks post-implantation, mice received 70 mg STZ per kilogram body weight (Sigma, S0130), through intraperitoneal injection for 5 consecutive days for a total dose of 350 mg/kg. When implanted animals reached blood glucose levels higher than 300 mg/dL for at least 7 consecutive days, the animals were euthanized.

Ex Vivo Histological Analysis

Encapsulation devices were retrieved and fixed in 4% paraformaldehyde for 4–7 days, dehydrated, and processed for paraffin embedding. Samples were sliced on a microtome at a thickness of 5 μm and stained with H&E. Insulin staining was revealed by immunohistochemistry using human insulin antibody (Dako, A0564) and images were acquired with a bright-field microscope (Leica) with a 10× objective (Supplemental Information).

Human Islets Preparation

Human islets from non-diabetic deceased donors were purchased from tebu-bio, providing donor consent forms for medical research. Islets were cultured at 37°C in a humidified atmosphere (5% CO_2). Details on culture medium are provided in Supplemental Experimental Procedures. Human islets were sampled after a maximum 4 days in culture for RNA analyses. All human islet procedures were approved by Comission cantonal d'étique de la recherche sur l'être humain (306/14).

Gene Expression Analyses

Total RNA from aggregates, human islets, or explanted tissue was isolated, quantified, and qualified using specific commercial kits (detailed information in Supplemental Experimental Procedures). Gene expression analysis was performed using the NanoString nCounter gene expression assay with100 ng RNA per reaction and the Combo_6980 code set according to the manufacturer's instructions (NanoString). Detailed information on code set and analysis of the data are provided in Supplemental Experimental Procedures. The average and standard deviations of the fully normalized counts were calculated for two biological replicates.

Immunofluorescence and High Content Image Analyses

D12 aggregates or explants were cryopreserved and embedded in 7.5% gelatin (details provided in Supplemental Experimental Procedures). The whole explant/aggregates were sectioned at −28°C in 4 μm thick sections using a microtome, and for each staining, tissue was analyzed every 40 μm. Immunofluorescence was performed using standard methods detailed in Supplemental Experimental Procedures. Details of primary and secondary antibodies are listed in Table S2. Images were acquired with an Axio Imager M2 Zeiss microscope. For high content image analyses and quantifications, whole slide images were acquired using an Olympus Slide Scanner (VS120-SL) with a 10× objective, which is suitable for quantification. Quantification was done using MetaXpress. Details of quantifications are provided as Supplemental Experimental Procedures.

Flow Cytometry Analyses

Single-cell suspensions of D12 HiPECs were obtained by dissociating cells with Accumax (Innovative Cell Technologies, AM105) at 37°C for 15 min. Live/dead staining (Thermo Fisher L34963) was performed for 20 min at room temperature. For intracellular antibody staining, cells were fixed using Fix/Perm buffer (Bioscience, 00-5523-00) for 30 min at room temperature and then washed with Perm buffer. Cells were re-suspended in 100 μL Perm/Wash buffer and then incubated overnight at 4°C with 50 μL primary antibodies mix. Details of antibodies are listed in Table S3. Dead cells were excluded during flow cytometry analysis and gating was determined using isotype antibodies. Flow cytometry data were acquired on a Becton Dickinson FACS FORTESSA and analyzed using De Novo FCS express software.

Glucose-Stimulated C-Peptide Secretion Assay and Intraperitoneal Glucose Tolerance Assays

Following overnight fasting, animals received an intraperitoneal injection of a 30% glucose (dextrose) solution dosed at 3.0 g/kg body weight. Blood samples were collected before and following the glucose injection at 15, 30, and 60–120 min. To evaluate the c-peptide release *ex vivo*, the explants were retrieved from the devices. Human c-peptide concentration in sera or supernatant samples was determined using the Ultrasensitive Human c-peptide ELISA as described by the manufacturer (Mercodia, 10-1141-01). Blood glucose levels were measured with glucometer strips and the glucometer Accu-Chek (Aviva).

Calcium Signaling Analyses

Explants were partially digested with Accumax at 37°C and plated on 35 mm diameter glass-bottom dishes (MatTek, P35G-1.5-20-C) coated with 804G matrix (Langhofer et al., 1993) in medium

composition. Experiments were performed 48 h post-transfection, at 37°C in Krebs-Ringer bicarbonate HEPES buffer (detailed in Supplemental Experimental Procedures). Glass coverslips were inserted into a thermostatic chamber (Life Imaging Services). Cells were excited at 430 nm and imaged on a DMI6000 B inverted fluorescence microscope, using an HCX PL APO 40×/1.30 NA oil immersion objective (Leica Microsystems) and an Evolve 512 back-illuminated CCD with 16 × 16 pixels camera (Photometrics) (details in Supplemental Experimental Procedures). Images were acquired every 2 s.

SUPPLEMENTAL INFORMATION

Supplemental Information includes Supplemental Experimental Procedures, six figures, and three tables and can be found with this article online at https://doi.org/10.1016/j.stemcr.2019.02.002.

AUTHOR CONTRIBUTIONS

C.H. and J.P. designed the study, developed protocols, analyzed data, and contributed to the manuscript. F.D-F. designed the study, developed protocols, and analyzed data. Y.O. and A.B. developed protocols and analyzed data. U.D-M. performed calcium signaling experiments, analyzed data, and contributed to the manuscript. C.B. performed encapsulation devices and cell encapsulation. G.J. developed the image analysis program for the scanning imaging. S.M. performed NanoString experiments. P.D. contributed to the manuscript. A.W. contributed to the manuscript. A.P. designed flow cytometry experiments. N.B. developed technology on encapsulation devices. P.S. contributed to the manuscript. O.G.K. contributed to the study design and to the manuscript. M.R-C.K. designed the study, analyzed data, and wrote the manuscript. M.R-C.K. is the guarantor of this work and, as such, had full access to all the data in the study and takes responsibility for the integrity of the data and the accuracy of the data analysis.

ACKNOWLEDGMENTS

REFERENCES

Bruin, J.E., Asadi, A., Fox, J.K., Erener, S., Rezania, A., and Kieffer, T.J. (2015). Accelerated maturation of human stem cell-derived pancreatic progenitor cells into insulin-secreting cells in immuno-deficient rats relative to mice. Stem Cell Reports 5, 1081–1096.

Castaing, M., Peault, B., Basmaciogullari, A., Casal, I., Czernichow, P., and Scharfmann, R. (2001). Blood glucose normalization upon transplantation of human embryonic pancreas into beta-cell-deficient SCID mice. Diabetologia 44, 2066–2076.

D'Amour, K.A., Agulnick, A.D., Eliazer, S., Kelly, O.G., Kroon, E., and Baetge, E.E. (2005). Efficient differentiation of human embryonic stem cells to definitive endoderm. Nat. Biotechnol. 23, 1534–1541.

D'Amour, K.A., Bang, A.G., Eliazer, S., Kelly, O.G., Agulnick, A.D., Smart, N.G., Moorman, M.A., Kroon, E., Carpenter, M.K., and Baetge, E.E. (2006). Production of pancreatic hormone-expressing endocrine cells from human embryonic stem cells. Nat. Biotechnol. 24, 1392–1401.

De Marchi, U., Thevenet, J., Hermant, A., Dioum, E., and Wiederkehr, A. (2014). Calcium co-regulates oxidative metabolism and ATP synthase-dependent respiration in pancreatic beta cells. J. Biol. Chem. 289, 9182–9194.

Dominguez-Bendala, J., Lanzoni, G., Klein, D., Alvarez-Cubela, S., and Pastori, R.L. (2016). The human endocrine pancreas: new insights on replacement and regeneration. Trends Endocrinol. Metab. 27, 153–162.

Franz, S., Rammelt, S., Scharnweber, D., and Simon, J.C. (2011). Immune responses to implants—a review of the implications for the design of immunomodulatory biomaterials. Biomaterials 32, 6692–6709.

Gaber, A.O., Fraga, D., Kotb, M., Lo, A., Sabek, O., and Latif, K. (2004). Human islet graft function in NOD-SCID mice predicts clinical response in islet transplant recipients. Transplant. Proc. 36, 1108–1110.

Haller, C., Chaskar, P., Piccand, J., Cominetti, O., Macron, C., Dayon, L., and Kraus, M.R. (2018). Insights into islet differentiation and maturation through proteomic characterization of a human iPSC-derived pancreatic endocrine model. Proteomics Clin. Appl. 12, e1600173.

Hering, B.J., Kandaswamy, R., Ansite, J.D., Eckman, P.M., Nakano, M., Sawada, T., Matsumoto, I., Ihm, S.H., Zhang, H.J., Parkey, J., et al. (2005). Single-donor, marginal-dose islet transplantation in patients with type 1 diabetes. JAMA 293, 830–835.

Jiang, W., Shi, Y., Zhao, D., Chen, S., Yong, J., Zhang, J., Qing, T., Sun, X., Zhang, P., Ding, M., et al. (2007). In vitro derivation of functional insulin-producing cells from human embryonic stem cells. Cell Res. 17, 333–344.

Kelly, O.G., Chan, M.Y., Martinson, L.A., Kadoya, K., Ostertag, T.M., Ross, K.G., Richardson, M., Carpenter, M.K., D'Amour, K.A., Kroon, E., et al. (2011). Cell-surface markers for the isolation of pancreatic cell types derived from human embryonic stem cells. Nat. Biotechnol. 29, 750–756.

Kirk, K., Hao, E., Lahmy, R., and Itkin-Ansari, P. (2014). Human embryonic stem cell derived islet progenitors mature inside an encapsulation device without evidence of increased biomass or cell escape. Stem Cell Res. 12, 807–814.

Kroon, E., Martinson, L.A., Kadoya, K., Bang, A.G., Kelly, O.G., Eliazer, S., Young, H., Richardson, M., Smart, N.G., Cunningham, J., et al. (2008). Pancreatic endoderm derived from human embryonic

stem cells generates glucose-responsive insulin-secreting cells in vivo. Nat. Biotechnol. *26*, 443–452.

Kumagai-Braesch, M., Jacobson, S., Mori, H., Jia, X., Takahashi, T., Wernerson, A., Flodstrom-Tullberg, M., and Tibell, A. (2013). The TheraCyte device protects against islet allograft rejection in immunized hosts. Cell Transplant. *22*, 1137–1146.

Langhofer, M., Hopkinson, S.B., and Jones, J.C. (1993). The matrix secreted by 804G cells contains laminin-related components that participate in hemidesmosome assembly in vitro. J. Cell Sci. *105* (Pt 3), 753–764.

Lathuiliere, A., Cosson, S., Lutolf, M.P., Schneider, B.L., and Aebischer, P. (2014). A high-capacity cell macroencapsulation system supporting the long-term survival of genetically engineered allogeneic cells. Biomaterials *35*, 779–791.

Lee, S.H., Hao, E., Savinov, A.Y., Geron, I., Strongin, A.Y., and Itkin-Ansari, P. (2009). Human beta-cell precursors mature into functional insulin-producing cells in an immunoisolation device: implications for diabetes cell therapies. Transplantation *87*, 983–991.

Matsuoka, T.A., Artner, I., Henderson, E., Means, A., Sander, M., and Stein, R. (2004). The MafA transcription factor appears to be responsible for tissue-specific expression of insulin. Proc. Natl. Acad. Sci. U S A *101*, 2930–2933.

Matveyenko, A.V., Georgia, S., Bhushan, A., and Butler, P.C. (2010). Inconsistent formation and nonfunction of insulin-positive cells from pancreatic endoderm derived from human embryonic stem cells in athymic nude rats. Am. J. Physiol. Endocrinol. Metab. *299*, E713–E720.

Millman, J.R., Xie, C., Van Dervort, A., Gurtler, M., Pagliuca, F.W., and Melton, D.A. (2016). Generation of stem cell-derived beta-cells from patients with type 1 diabetes. Nat. Commun. *7*, 11463.

Motte, E., Szepessy, E., Suenens, K., Stange, G., Bomans, M., Jacobs-Tulleneers-Thevissen, D., Ling, Z., Kroon, E., and Pipeleers, D.; Beta Cell Therapy Consortium EU-FP7 (2014). Composition and function of macroencapsulated human embryonic stem cell-derived implants: comparison with clinical human islet cell grafts. Am. J. Physiol. Endocrinol. Metab. *307*, E838–E846.

Nostro, M.C., Sarangi, F., Ogawa, S., Holtzinger, A., Corneo, B., Li, X., Micallef, S.J., Park, I.H., Basford, C., Wheeler, M.B., et al. (2011). Stage-specific signaling through TGFbeta family members and WNT regulates patterning and pancreatic specification of human pluripotent stem cells. Development *138*, 861–871.

Nostro, M.C., Sarangi, F., Yang, C., Holland, A., Elefanty, A.G., Stanley, E.G., Greiner, D.L., and Keller, G. (2015). Efficient generation of NKX6-1+ pancreatic progenitors from multiple human pluripotent stem cell lines. Stem Cell Reports *4*, 591–604.

Pagliuca, F.W., Millman, J.R., Gurtler, M., Segel, M., Van Dervort, A., Ryu, J.H., Peterson, Q.P., Greiner, D., and Melton, D.A. (2014). Generation of functional human pancreatic beta cells in vitro. Cell *159*, 428–439.

Rezania, A., Bruin, J.E., Arora, P., Rubin, A., Batushansky, I., Asadi, A., O'Dwyer, S., Quiskamp, N., Mojibian, M., Albrecht, T., et al. (2014). Reversal of diabetes with insulin-producing cells derived in vitro from human pluripotent stem cells. Nat. Biotechnol. *32*, 1121–1133.

Rezania, A., Bruin, J.E., Riedel, M.J., Mojibian, M., Asadi, A., Xu, J., Gauvin, R., Narayan, K., Karanu, F., O'Neil, J.J., et al. (2012). Maturation of human embryonic stem cell-derived pancreatic progenitors into functional islets capable of treating pre-existing diabetes in mice. Diabetes *61*, 2016–2029.

Robert, T., De Mesmaeker, I., Stange, G.M., Suenens, K.G., Ling, Z., Kroon, E.J., and Pipeleers, D.G. (2018). Functional beta cell mass from device-encapsulated hESC-derived pancreatic endoderm achieving metabolic control. Stem Cell Reports *10*, 739–750.

Russ, H.A., Parent, A.V., Ringler, J.J., Hennings, T.G., Nair, G.G., Shveygert, M., Guo, T., Puri, S., Haataja, L., Cirulli, V., et al. (2015). Controlled induction of human pancreatic progenitors produces functional beta-like cells in vitro. EMBO J. *34*, 1759–1772.

Schulz, T.C. (2015). Concise review: manufacturing of pancreatic endoderm cells for clinical trials in type 1 diabetes. Stem Cells Transl. Med. *4*, 927–931.

Schulz, T.C., Young, H.Y., Agulnick, A.D., Babin, M.J., Baetge, E.E., Bang, A.G., Bhoumik, A., Cepa, I., Cesario, R.M., Haakmeester, C., et al. (2012). A scalable system for production of functional pancreatic progenitors from human embryonic stem cells. PLoS One *7*, e37004.

Shapiro, A.M. (2011). State of the art of clinical islet transplantation and novel protocols of immunosuppression. Curr. Diab. Rep. *11*, 345–354.

Shapiro, A.M., Lakey, J.R., Ryan, E.A., Korbutt, G.S., Toth, E., Warnock, G.L., Kneteman, N.M., and Rajotte, R.V. (2000). Islet transplantation in seven patients with type 1 diabetes mellitus using a glucocorticoid-free immunosuppressive regimen. N. Engl. J. Med. *343*, 230–238.

Tuch, B.E., Monk, R.S., and Beretov, J. (1991). Reversal of diabetes in athymic rats by transplantation of human fetal pancreas. Transplantation *52*, 172–175.

Vegas, A.J., Veiseh, O., Gurtler, M., Millman, J.R., Pagliuca, F.W., Bader, A.R., Doloff, J.C., Li, J., Chen, M., Olejnik, K., et al. (2016). Long-term glycemic control using polymer-encapsulated human stem cell-derived beta cells in immune-competent mice. Nat. Med. *22*, 306–311.

Yang, H., and Wright, J.R., Jr. (2002). Human beta cells are exceedingly resistant to streptozotocin in vivo. Endocrinology *143*, 2491–2495.

Zhang, C., Moriguchi, T., Kajihara, M., Esaki, R., Harada, A., Shimohata, H., Oishi, H., Hamada, M., Morito, N., Hasegawa, K., et al. (2005). MafA is a key regulator of glucose-stimulated insulin secretion. Mol. Cell. Biol. *25*, 4969–4976.

Zhang, D., Jiang, W., Liu, M., Sui, X., Yin, X., Chen, S., Shi, Y., and Deng, H. (2009). Highly efficient differentiation of human ES cells and iPS cells into mature pancreatic insulin-producing cells. Cell Res. *19*, 429–438.